Journal of Ovonic Research Vol. 20, No. 3, May - June 2024, p. 357 - 364

Electrochemical performance of rice grains like high Mn-doped anatase TiO_2 nanoparticles as lithium-ion batteries electrode material

H. Q. Zhao*, L. Li, Q. S. Yuan
Northeast Petroleum University, Department of petroleum and chemical engineering, Qinhuangdao 066004, Hebei Province, China

Rice grain-shaped high Mn-doped anatase TiO_2(TMO) nanocrystals have been fabricated through redox method at room temperature using several simple chemical reagents. The samples were characterized by X-ray diffraction (XRD), X-ray photoelectron spectroscopy(XPS), scanning electron microscopy(SEM), transmission electron microscopy and High-resolution transmission electron microscopy (TEM & HRTEM). It indicates that the manganese element was successfully incorporated into the anatase TiO_2 nanostructure, and the atomic Mn-to-Ti could reach up to 18.2%. We also analyzed the merits and weaknesses of the nanostructured TMO in electrochemistry by dint of some relevant measures. And the cause of influence on the TMO electrochemical properties was briefly discussed.

(Received February 24, 2024; Accepted May 27, 2024)

Keywords: Mn-doped TiO_2, Nano material, Lithium-ion, Electrochemical properties

1. Introduction

Nowadays more and more attentions are paid for the field of new energy and environment, particularly Lithium-ion batteries as the substitute of fossil fuel such as coal, oil, natural gas etc. In rechargeable lithium-ion batteries, anode materials as one of the key components, mainly devotes to the performance of the batteries. Because of large surface area and tunable pore size, titanium dioxide (TiO_2) usually as anode material show up high reactivity, inherent chemical stability and prompt response on energy applications as well as abundance in resources for safer and cost-efficient batteries. [1,2] The theoretical specific capacity of TiO_2 is 335 $mAhg^{-1}$, close to the commercial graphite theoretical specific capacity (372 $mAhg^{-1}$). But because of the poor electron conductivity and other factors, the real performance of the capacity is limited, and can't meet the demand of the development of high-capacity lithium battery. Doping heterogeneous element or varying bulk TiO_2 materials to nanoscale is believed two promising methods as it could enable TiO_2 to improve Li insertion sites and electron transfer ability. Wang et al, reported that the tungsten doped anatase TiO_2(WTO) nanoparticles with high surface area has been prepared and the highly stable capacity of 170 $mAhg^{-1}$ has been found after 100 cycles.[3] As one of the most attractive inorganic materials in recently years, manganese dioxide (MnO_2) is an important functional metal oxide because of its physical and chemical properties and wide applications in catalysis, ion

* Corresponding author: 261981010228@nepu.edu.cn
https://doi.org/10.15251/JOR.2024.203.357

exchange, and particularly in energy storage.[4-6] In a general way, metallic manganese is difficult to dope other metal or metal oxide particles. But as known to all, the basic structure unit (namely, the [MnO_6] octahedron) of MnO_2 is very similar to the [TiO_6] octahedron of TiO_2, it may be meaning that manganese element enters easily into the TiO_2 crystal lattice. In addition, the uptake of Li^+ has been found to be much better in anatase lattice than in rutile structures in general.[7]

Here, a simple method for preparing high Mn-doped anatase TiO_2 to improve the electrochemical properties of TiO_2 is described. Titanium gel using metallic titanium and hydrogen peroxide have been previously prepared.[8,9] Our method is based on the titanium gel reacting with the block of manganese sesquioxide, then TMO is obtained with small particle sizes and good crystallinity. The as-prepared samples is used as anode for lithium-ion batteries, and its charge-discharge properties are examined. We also compare TO nanoparticles with it at the same loading conditions.

2. Experimental

2.1. Synthesis

Commercial Ti powders (99.5% purity, 45 μm in average size) as the original materials was weighed in duplicate, and then respectively devolved into a beaker which filled with 500 mL 30% H_2O_2 to produce an acidic solution at room temperature. One beaker was put in an oven and dried under conditions of 80℃.The nanostructured anatase TO powder was obtained. Mn_2O_3 block (fired from Mn_2O_3 powder, purchased from alpha) was added to another beaker for reacting about 12 hours. When the reaction was finished, the Mn_2O_3 block was removed off, and the beaker transferred to an oven dried under the conditions of 80℃, then the nanostructured TMO powder was obtained.

2.2. Characteration

High-resolution transmission electron microscopy (HRTEM) samples were prepared by evaporation of the TMO powder in acetone or hexane on carbon-coated copper grids. The field-emission electron microscope was a JEM-2010 (JEOL, Japan) operating at 200 kV. Powder X-ray diffraction (XRD) measurements were carried out using a Rigaku D/Max-2500PC (Japan) with a Cu-target tube at 40 mA and 40 kV. Morphologies of the powders were checked using a field-emission scanning electron microscopy (SEM) (Model S4800, HITACHI, Japan). X-ray photoelectron spectroscopy (XPS) was used to measure the composition and the valence states of the TMO nanoparticles with Al Kα radiation of 1486.6 eV in ESCALAB 250xi (Thermo Fisher Scientific).

Anode for the battery test cells were made of the TMO nanopowders, carbon black, and polyvinylidene fluoride (PVDF) binder (Solef) in the weight ratio of 80:10:10. The slurry was prepared by thoroughly mixing an N-methyl-2-pyrrolidone (NMP) (Aldrich) solution of the TMO nanopowders, PVDF, and carbon black, and then pasted onto a Cu foils (Ø = 16 mm). The coin-type cells were assembled in an argon-filled Mikrouna glovebox, where both moisture and oxygen levels were less than 1 ppm, contained the Cu foils, a Li metal cathode, a microporous polyethylene separator, and an electrolyte solution of 1 M $LiPF_6$ in 1:1 v/v ethylene carbonate/dimethyl carbonate (EC/DMC) (Cheil Industries, Korea). The mass loading was around 1.0 mg.

3. Results and discussion

3.1. Structural and morphology

The XRD pattern of TO and TMO shown in Fig.1a is similar to that of TiO_2 (anatase type, space group $I4_1/amd$) and can be indexed as tetragonal lattice. It is clearly evident that the formation of a single phase, which is suggested by all of reflections in both lines, and the well-developed diffraction line of anatase TMO has none of crystalline byproducts, such as MnO_2 or Mn_2O_3. Being compared with TO, the (004) crystal peak moved to the right and having no (112) crystal peak in the TMO spectral lines, it is believed that the manganese doping occurred by substituting the titanium atom in the crystal structure. As a result of the existence of manganese ions, the (112) crystal plane of TMO crystal lattice is destroyed, and the manganese partially instead of titanium ions is further confirmed. Both (105) and (211) crystal peak was broadened into a peak, just as the (116) and (220) crystal peaks. It is believed to be caused by manganese-doped having the crystalline of the anatase TMO nanoparticles become poor. The morphology of rice grains like TMO nanostructures was characterized by SEM, as shown in Fig.1b. SEM image reveals that the microsphere particles are with the diameter of 15-30 nm and rough surface. It is demonstrated that TMO nanoparticles is endowed with small pore size and large surface area. When the TMO nanopowders are used as anode materials, Li insertion sites and electron transfer ability would be improved.

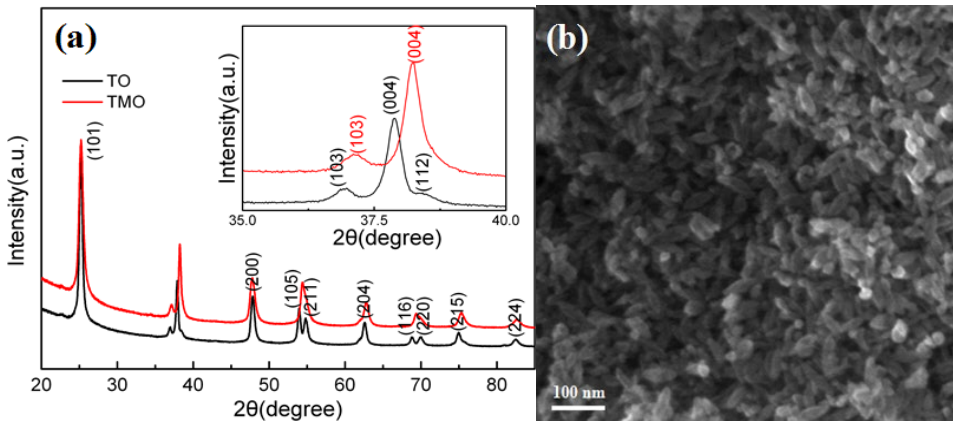

Fig. 1. The XRD pattern of TO and TMO nanoparticles.

With the help of the MAUD programs to analyse the XRD spectra,[10] the refined lattice parameters of tetragonal system are shown in Tab.1. The results showed that Mn doping made c and crystalline size decreasing: c value dropped from 0.944 nm to 0.942 nm, it is mean that the interlamellar spacing decreased and the interlayer structure may become more stable. Crystalline size also fell from 18.2 nm to 16.5 nm, indicates TMO nanopowders size becoming smaller, beneficial to the improvement of the electrochemical properties.

Table 1. Effect of Mn doping on the refined lattice parameters of tetragonal system.

	a(nm)	c(nm)	Crystalline size(nm)
TO	0.380	0.944	18.2
TMO	0.380	0.942	16.5

To investigate the composition and the valence states of the TMO nanoparticles, Ti 2p and Mn 2p core levels were measured by XPS analyses, which confirmed the chemical consisting solely of Ti, Mn and O of the TMO nanoparticles, as shown in Fig.2a and 2b. Two peaks of pure TiO_2 are 464.4 and 458.8 eV, and two peaks of pure MnO_2 are 653.8 and 642.1 eV, respectively.[11] But the Ti $2p_{1/2}$ and Ti $2p_{3/2}$ peak in Fig.2a positioned at 464.1 and 458.3 eV, and the Mn $2p_{1/2}$ and Mn $2p_{3/2}$ peak was 653.6 and 641.9 eV. It is because of the forming of Ti-O-Mn structure in TiO_2 lattice through substitution of manganese ion.[12] The result indicates that manganese atoms partly replace titanium atoms and its oxidation state is +4 as same as titanium atoms. The result of the atomic Mn-to-Ti ratio of 18.2% was gained from the analysis of XPS. It affirms that manganese element can enter easily into the TiO_2 crystal lattice.

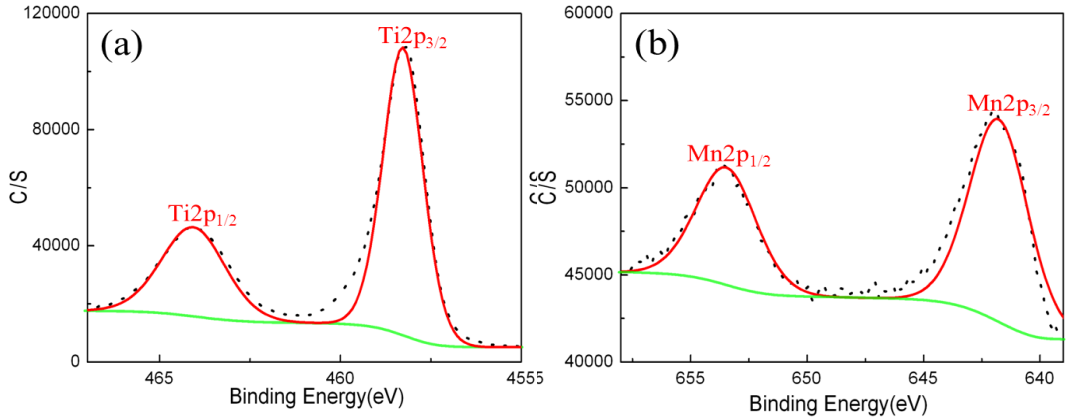

Fig. 2. The high-resolution XPS spectra of superposed Ti 2p (a) and Mn 2p (b) for the TMO nanoparticles.

By electron microscopy investigations, the uniform rice-like nanostructures of TMO were further confirmed. About 15-30 nm in diameter and 60-80 nm in length are showed in electron microscopy (TEM) image (Fig.3a). The crystallinity of the particles leads to its well pronounced Debye-Scherrer diffraction rings, in the corresponding selected-area electron diffraction (SEAD) pattern of an ensemble of the powder, from the inset in Fig.3a. As shown in Fig.3b, the high-resolution TEM (HRTEM) image reveals the good crystallinity of TMO nanocrystals. In comparison with the corresponding fast Fourier transform (FFT) pattern (inset of Fig.3b), the exposed surface of these as-prepared TMO nanocrystals are predominantly {101} and {004} facets. It is noted that the {101} facets are well developed and flat, while the {004} facets are less developed and curved. The same constructed structure model, as the high-resolution TEM (HRTEM) image in Fig.3b, viewed along the direction of [001] zone-axis was shown in the inset of Fig.3b.

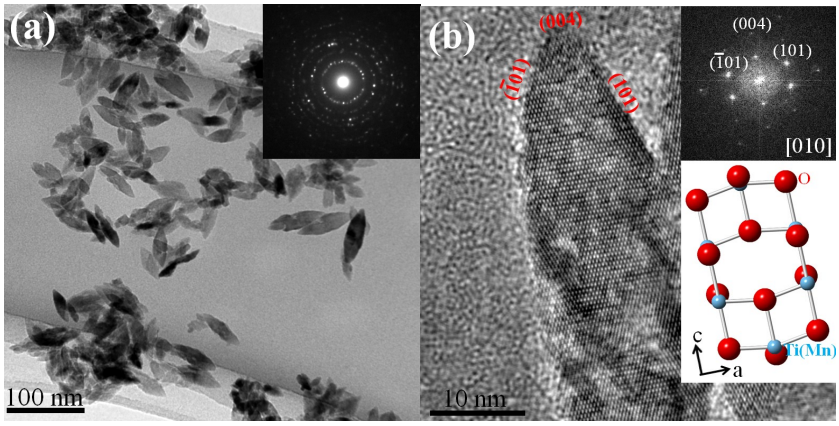

Fig. 3. (a) TEM image and (b) HRTEM image of TMO nanoparticles.

3.2 Electrochemical studies

The initial charge-discharge curves of the TO and TMO nanoparticles electrodes were presented in Fig.4a. As can be seen, both of the discharge or charge voltages (TO or TMO) started forming two distinct discharge or charge potential plateaus near 1.73 V or 1.88 V as the representative one of electrochemical lithium insertion or extraction of anatase-type TiO_2, which is further evidence of the preparation of the TO and TMO nanoparticles with anatase structure.[13] When the charge-discharge current density was 30 mAg^{-1}, the first discharge capacity of the TMO nanoparticles could reach 679 $mAhg^{-1}$, is larger than the TO nanoparticles (629 $mAhg^{-1}$). The first charge curve of TO and TMO in the range of 0 - 1.88 V is approximately a straight line, and the slope of TMO is smaller than the one of TO, it most probably indicates that the charge speed of TMO is much faster than the TO, and it is believed to be caused by manganese-doped making the electrical conductivity of the anatase TMO nanoparticles improved. When the charging process was over, the first charge capacity (213 $mAhg^{-1}$) was larger than the TO (179 $mAhg^{-1}$), it is certain that the charging capacity is increased in the TMO Li-batteries after manganese doping.

Charge-discharge capacity of TO and TMO versus cycle numbers were given in Fig.4b. In both curves of TO and TMO, a distinct drop of irreversible capacity could be found until the top 20 cycles. The similar phenomena are also observed in other type of TiO_2, such as anatase, rutile, etc.[14,15] From 20 cycles to 50 cycles, the charge capacity of TO still kept ratcheting downward，it is because of the poor conductive performance of TiO_2.[16] The charge capacity of TMO as a whole also presented less downtrend obvious. It may be caused by the side reaction arising from the catalytic properties of the variable price elements like titanium and manganese. It may also be affected by the surface defects of TMO, or by becoming locked within the crystal structure for lattice stabilization purposes.[17,18] But after 30 cycles there was a small growth to stable the charge-discharge capacity and the charge capacity of TMO was kept. After 50 cycles, the stable TMO capacity of 91.6 $mAhg^{-1}$ was superior to the TO capacity of 26.7 $mAhg^{-1}$, but it was inferior to the capacity of W-doped anatase TiO_2 nanoparticles of the kind mentioned. We conjecture that despite manganese doping improves the conductivity of anatase TiO_2 by doping heterogeneous elements, manganese ion is much smaller than titanium ion. It means that manganese doping makes the interlamellar spacing decreased so small that the lithium ion can difficultly enter into it. This is the opposite of tungsten ion. Because the purpose of this study is to investigate the electrochemical performance of

Mn-doped anatase TiO_2 (TMO) nanoparticles, we did not research the affection of ionic radius. However, we are deciding to execute this aspect of studies to make it clear.

The charge-discharge current densities in the range of 30 mAg^{-1} to 960 mAg^{-1} have been investigated and the corresponding results are shown in Fig.4c. The discharge capacity was basically stable of about 174 $mAhg^{-1}$ at current density of 30 mAg^{-1}. It approximately reduced to 127 $mAhg^{-1}$ at 60 mAg^{-1}, 99 $mAhg^{-1}$ at 120 mAg^{-1}, 75 $mAhg^{-1}$ at 240 mAg^{-1}, 54 $mAhg^{-1}$ at 480 mAg^{-1}, and finally, 34 $mAhg^{-1}$ at 960 mAg^{-1}. After this complete dynamic loading cycle, the first charge capacity of 128 $mAhg^{-1}$ was obtained by returning to the current density of 30 mAg^{-1} for a second time, it indicates that the preferable cycling stability of the TMO nanoparticles even after rather harsh charge-discharge current densities.

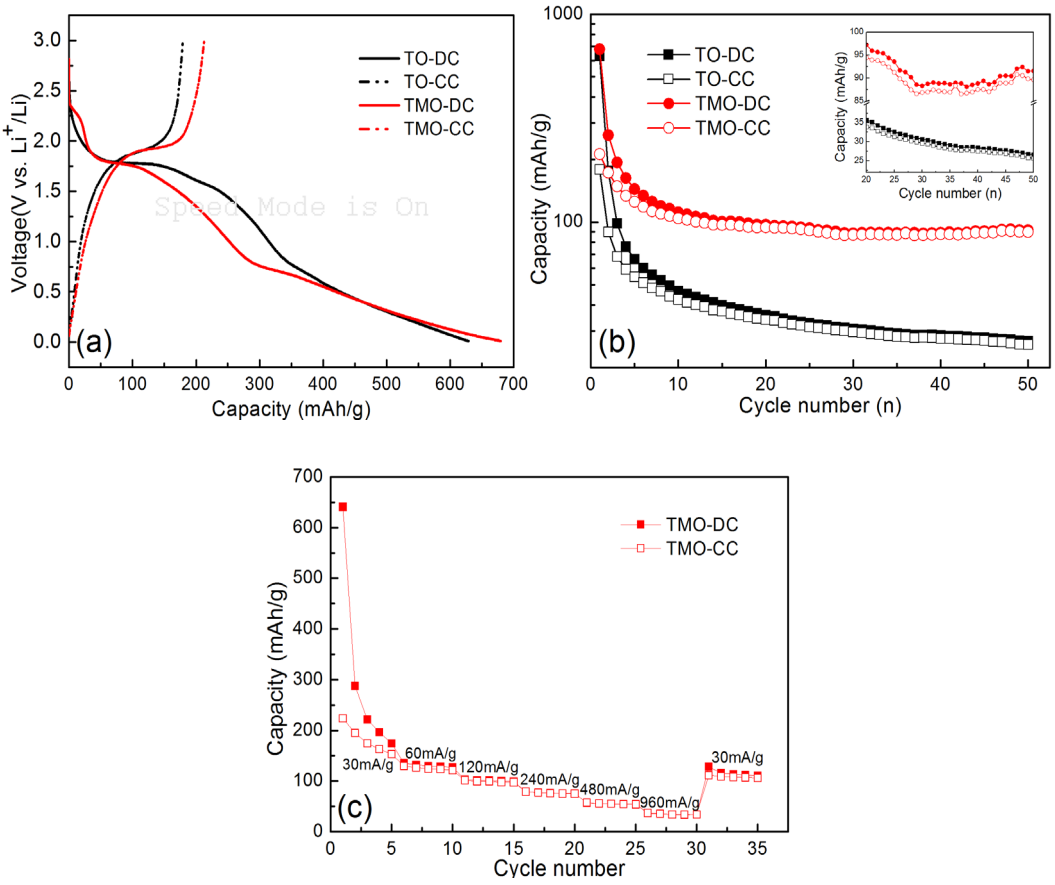

Fig. 4. (a) The galvanostatic voltage profiles of TO and TMO between 0 V and 3 V for the first cycle, (b) the charge/discharge performance of TO and TMO during the top 50 cycles at 30 mAg^{-1}, and (c) the charge/discharge performance of TMO during the different charge/discharge current density.

4. Conclusions

Rice grain-shaped high Mn-doped anatase TiO_2 nanoparticles with large surface area and good crustal structure were synthesized through redox method at room temperature. The XRD, TEM (HRTEM) and XPS results confirms that the manganese is successfully incorporated into the anatase

TiO_2 nanostructure. The XPS results further show that the atomic Mn-to-Ti is of 18.2%, which means that the manganese can enters easily into the TiO_2 crystal lattice and has a heavy doping. The good electrochemical performance of TMO as a anode for a lithium battery was shown.

At the constant discharge current density of 30 mAg^{-1}, its first discharge capacity about 679 $mAhg^{-1}$ could be obtained in the potential range of 0-3 V. In comparison with the charge-discharge capacity of TO after 20 cycles, the charge-discharge capacity of TMO straight keep less downtrend obvious. Since about 30 cycles, unexpectedly, there is a little increase to stable the TMO capacity. It is well illustrated that doping TiO_2 with manganese element and varying bulk TiO_2 materials to nanoscale is important for electrochemical lithium storage.

Acknowledgements

This research was supported by the Guided Innovation Fund of Northeast Petroleum University (Grant No. 2021YDQ-07) and the Qinhuangdao Science and Technology Research and Development Program (Grant No. 202101A206).

References

[1] W. Zhang, Y. Tian, H. L. He, L. Xu, W. Li, D. Y. Zhao, National Science Review, 7(11), 1702(2020); https://doi.org/10.1093/nsr/nwaa021
[2] S. Z. Liang, X. Y. Wang, R. X. Qi, Y. J. Cheng, Y. G. Xia, P. M. Buschbaum, X. L. Hu, Advanced Functional Materials, 32(25), 2201675(2022); https://doi.org/10.1002/adfm.202201675
[3] Y. D. Wang, T. Chen, Q. Y. Mu, Journal of Materials Chemistry, 21(16), 6006(2011); https://doi.org/10.1039/C0JM04275G
[4] A. Debart, A. J. Paterson, J. L. Bao, P. G. Bruce, Angewandte Chemie, 120(24), 4597(2008); https://doi.org/10.1002/ange.200705648
[5] K. Wickramaarachchi, M. Minakshi, Journal of Energy Storage, 56, 106099(2022); https://doi.org/10.1016/j.est.2022.106099
[6] X. L. Ye, D. L. Han, G. Y. Jiang, C. J. Cui, Y. Guo, Y. G. Wang, Z. C. Zhang, Z. Weng, and Q. H. Yang, Energy & Environmental Science, 16(3), 1016(2023); https://doi.org/10.1039/D3EE00018D
[7] J. Y. Kim, J. Cho, Journal of The Electrochemical Society, 154 (6), 542(2007); https://doi.org/10.1149/1.2724756
[8] P. Tengvall, H. Elwing, and I. Lundstrom. Journal of Colloid and Interface Science, 130(2), 405(1989); https://doi.org/10.1016/0021-9797(89)90117-3
[9] P. Tengvall, L. Bertilsson, B. Liedberg, H. Elwing, I. Lundstrom. Journal of Colloid and Interface Science, 139(2), 575(1990); https://doi.org/10.1016/0021-9797(90)90131-7
[10] L. Luca, S. Matthies, H. Wenk, CPD Newsletter, 21(2), (1999); https://hdl.handle.net/11572/38076
[11] J. F. Moulder, W. F. Stickle, P. E. Sobol, K. D. Bomben, Handbook of X-ray Photoelectron Spectroscopy, published by Perkin-Elmer Corporation Physical Electronics Division. Eden Prairie, Minnesota, 78-79(1992).

[12] L. Pan, J. J. Zou, X. W. Zhang, L. Wang, Industrial & Engineering Chemistry Research, 49(18), 8526 (2010); https://doi.org/10.1021/ie100841w
[13] J. W. Xu, C. H. Jia, B. Cao, W. F. Zhang, Electrochimica Acta, 52(28), 8044(2007); https://doi.org/10.1016/j.electacta.2007.06.077
[14] G. Sudant, E. Baudrin, D. Larcher, J. M. Tarascon, Journal of Materials Chemistry, 15(12), 1263(2005); https://doi.org/10.1039/B416176A
[15] Y. S. Hu, L. Kienle, Y. G. Guo, J. Mater, Advanced Materials, 18(11), 1421(2006); https://doi.org/10.1002/adma.200502723
[16] C. Cai, Z. J. Yao, J. Y. Xiang, et al., Electrochimica Acta, 452, 142323(2023); https://doi.org/10.1016/j.electacta.2023.142323
[17] G. F.Ortiz, I. Hanzu, T. Djenizian, P. Lavela, J. L. Tirado, P. Knauth, Chemistry of Materials, 21(1), 63(2009); https://doi.org/10.1021/cm801670u
[18] M.Sugantha, P. A. Ramakrishnan, A. M. Hermann, C. P. Warmsingh, D. S. Ginley, International Journal of Hydrogen Energy, 28(6), 597(2003); https://doi.org/10.1016/S0360-3199(02)00148-9